doi:10.1038/nature09358

ARTICLES

MICU1 encodes a mitochondrial EF hand protein required for Ca^{2+} uptake

Fabiana Perocchi[1], Vishal M. Gohil[1], Hany S. Girgis[1], X. Robert Bao[1], Janet E. McCombs[2], Amy E. Palmer[2] & Vamsi K. Mootha[1]

Mitochondrial calcium uptake has a central role in cell physiology by stimulating ATP production, shaping cytosolic calcium transients and regulating cell death. The biophysical properties of mitochondrial calcium uptake have been studied in detail, but the underlying proteins remain elusive. Here we use an integrative strategy to predict human genes involved in mitochondrial calcium entry based on clues from comparative physiology, evolutionary genomics and organelle proteomics. RNA interference against 13 top candidates highlighted one gene, *CBARA1*, that we call hereafter mitochondrial calcium uptake 1 (*MICU1*). Silencing *MICU1* does not disrupt mitochondrial respiration or membrane potential but abolishes mitochondrial calcium entry in intact and permeabilized cells, and attenuates the metabolic coupling between cytosolic calcium transients and activation of matrix dehydrogenases. MICU1 is associated with the mitochondrial inner membrane and has two canonical EF hands that are essential for its activity, indicating a role in calcium sensing. MICU1 represents the founding member of a set of proteins required for high-capacity mitochondrial calcium uptake. Its discovery may lead to the complete molecular characterization of mitochondrial calcium uptake pathways, and offers genetic strategies for understanding their contribution to normal physiology and disease.

The uptake of calcium (Ca^{2+}) by vertebrate mitochondria was first documented nearly 50 years ago[1,2]. These early studies revealed that suspensions of isolated mitochondria can transport and buffer massive amounts of Ca^{2+} across the inner membrane. This high-capacity 'uniporter' mechanism is classically defined by its dependence on membrane potential, sensitivity to ruthenium red, and activity when extramitochondrial Ca^{2+} concentrations are in the micromolar range. Subsequent studies, using genetically encoded calcium indicators targeted to mitochondria[3–5], were crucial in establishing the physiological relevance of mitochondrial Ca^{2+} uptake in a variety of cell types.

It is now widely accepted that mitochondrial Ca^{2+} uptake can shape cytosolic Ca^{2+} signals and oscillations to regulate diverse physiological processes ranging from hormone secretion to cell differentiation[6,7]. Mitochondrial Ca^{2+} buffering seems to be particularly important at privileged microdomains near the ER and plasma membrane, where Ca^{2+} concentrations can reach high micromolar levels[8]. Mitochondrial Ca^{2+} uptake can stimulate TCA cycle dehydrogenases, providing a mechanism of 'feed-forward' control whereby Ca^{2+} signals ATP consumptive processes in the cytosol while also stimulating its production in mitochondria[9–11]. Excessive uptake of Ca^{2+}, however, can trigger the mitochondrial permeability transition, leading to cell death and contributing to pathogenesis[12].

Although the biophysical properties of mitochondrial Ca^{2+} uptake have been extensively characterized[13–15], the underlying molecular machinery has remained elusive. Several groups have reported the reconstitution of mitochondrial Ca^{2+} uptake activity in *in vitro* systems, yet none have identified the underlying proteins[16–18]. Because we lack specific, cell-permeant small molecules with which to interrogate these uptake pathways, it is difficult to evaluate rigorously how mitochondrial Ca^{2+} uptake impacts development and disease[15,19]. Furthermore, there are discrepancies between whole-cell, isolated mitochondria and electrophysiological studies of calcium uptake[15], and multiple transport mechanisms may exist[20,21], underscoring the need to characterize the underlying molecular machinery.

Here, we report a focused RNA interference (RNAi) strategy to identify mitochondrial proteins required for Ca^{2+} uptake based on clues from comparative physiology and organelle proteomics. Key to our approach is the observation that classically defined mitochondrial Ca^{2+} uniporter activity is evolutionarily conserved in vertebrates and in kinetoplastids[22–24], yet not measurable in the yeast *Saccharomyces cerevisiae*[22,25,26]. By searching for inner mitochondrial membrane proteins that share this evolutionary profile, we are able to prioritize a small number of human proteins that we then test using RNAi. Our strategy has enabled us to identify MICU1, a poorly characterized EF-hand-containing protein, which we now show is localized to the mitochondrion and required for mitochondrial Ca^{2+} uptake in HeLa cells.

Targeted RNAi screen

To prioritize proteins required for mitochondrial Ca^{2+} entry, we combined proteomic, physiological and evolutionary clues (see Methods). On the basis of decades of biochemical characterization, we expect the high-capacity, ruthenium-red-sensitive mitochondrial Ca^{2+} uptake machinery to be (1) localized to the mitochondrial inner membrane[1,2]; (2) expressed in the majority of mammalian tissues[22]; and (3) to have homologues in vertebrates[22] and kinetoplastids[23,24], but not in the yeast *S. cerevisiae*[22,25,26]. We began with MitoCarta, a proteomic inventory of 1,098 mouse mitochondrial proteins from 14 tissues, 1,013 of which we previously mapped to human genes[27]. Of the 1,013 human MitoCarta proteins, 18 fulfilled the above criteria as they have also been reported in purifications of the mitochondrial inner membrane[28,29], found in the majority of mammalian organs, and conserved to kinetoplastids but not in the yeast *S. cerevisiae*[27] (Fig. 1a). We prioritized 13 of these 18 genes for which RNAi reagents

[1]Center for Human Genetic Research, Massachusetts General Hospital, Boston, Massachusetts 02114, USA; Broad Institute, Cambridge, Massachusetts 02142, USA; Department of Systems Biology, Harvard Medical School, Boston, Massachusetts 02115, USA. [2]Department of Chemistry and Biochemistry, University of Colorado, Boulder, Colorado 80309, USA.

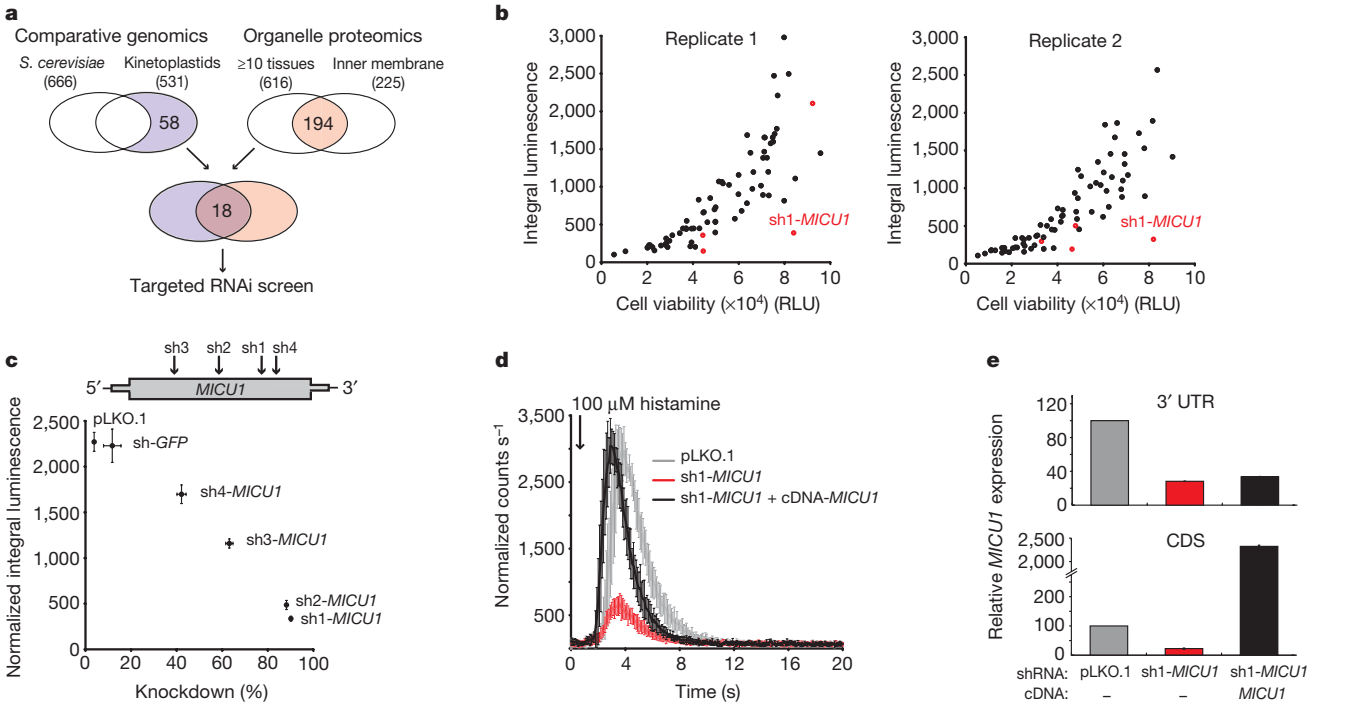

Figure 1 | Targeted RNAi screen for mitochondrial Ca^{2+} uptake. **a**, Integrative approach to predict human mitochondrial proteins involved in mitochondrial Ca^{2+} uptake. Numbers represent the subset of human MitoCarta genes with the indicated property. **b**, Targeted RNAi screen of mitochondrial Ca^{2+} uptake for 13 of the 18 top candidate genes. Each point represents one RNAi hairpin expressed in mt-AEQ HeLa cells. Mitochondrial Ca^{2+} uptake, reported as the integral luminescence over 30 s following 100 μM histamine stimulation, is plotted as a function of cell viability (relative luminescence units, RLU). RNAi hairpins targeting *MICU1* are shown in red. **c**, Relationship between mitochondrial Ca^{2+} uptake and *MICU1* knockdown. The region of the *MICU1* cDNA targeted by four distinct hairpins (sh1–sh4) is shown. Integral luminescence normalized to cell number (mean ± s.d., $n = 8$) is plotted as a function of *MICU1* gene expression relative to uninfected cells using actin as an endogenous control (mean ± s.d., $n = 3$). **d**, cDNA rescue of the sh1-*MICU1* mitochondrial Ca^{2+} phenotype. Kinetic traces of mitochondrial Ca^{2+} uptake normalized to cell number are shown for control cells (pLKO.1), *MICU1*-silenced cells and rescue cells (mean ± s.d., $n = 3$). **e**, Quantification of endogenous (3′ UTR) and endogenous + exogenous (CDS) *MICU1* expression in control, *MICU1* knockdown and cDNA rescue cells measured by qPCR. Relative gene expression is reported as percentage change over control cells (pLKO.1) using actin as an endogenous control (mean ± s.d., $n = 3$).

were available and which appeared to be the most plausible candidates.

We performed an RNAi screen of these top 13 candidates in a commercially available HeLa cell line (mt-AEQ) that stably expresses a mitochondria-targeted aequorin[3] (see Methods). Histamine stimulation of the reporter cell line leads to an inositol-1,4,5-trisphosphate ($Ins(1,4,5)P_3$)-triggered release of Ca^{2+} into the cytosol, some of which enters the mitochondria to trigger light emission[30]. Luminescence from mt-AEQ is influenced by the Ca^{2+} concentration within the mitochondrial matrix ($[Ca^{2+}]_m$), as well as by the number of viable cells in the population (Supplementary Fig. 1).

We used four or five short hairpin RNA (shRNA) constructs targeting each of the 13 genes and expressed them via lentiviral transduction in our reporter cell line (Supplementary Table 1). We sought to identify hairpins that attenuated mitochondrial Ca^{2+} uptake even after accounting for effects of the RNAi on cell number. The majority of candidate or control hairpins had no impact on mitochondrial Ca^{2+} uptake or only a secondary effect due to decreased cell number (Fig. 1b). However, one hairpin markedly reduced mitochondrial Ca^{2+} uptake independent of its effects on cell viability (Fig. 1). This hairpin corresponded to *CBARA1* (also known as *FLJ12684*), a hitherto poorly characterized gene, which we now rename as mitochondrial calcium uptake 1 (*MICU1*) (Fig. 1b). Next, we created four stable mt-AEQ HeLa cell lines in which we silenced the expression of *MICU1* using four distinct hairpins targeting the gene (Fig. 1c). The mitochondrial Ca^{2+} uptake phenotype showed a strong correlation to the strength of *MICU1* knockdown (Fig. 1c). It is notable that silencing of *MICU1* by the two most effective hairpins (sh1-*MICU1* and sh2-*MICU1*, giving 90% and 89% knockdown, respectively) resulted in similar Ca^{2+} phenotypes, although two distinct regions of the transcript had been targeted, indicating an on-target mechanism of action of these hairpins.

To formally exclude an off-target effect of sh1-*MICU1* on the mitochondrial Ca^{2+} phenotype, we performed a complementary DNA rescue study in *MICU1* knockdown cells. We engineered a hairpin-insensitive cDNA harbouring eight synonymous mutations within the sh1 target sequence and stably expressed it in sh1-*MICU1* knockdown cells via lentiviral transduction using orthogonal antibiotic selection (see Methods). As shown in Fig. 1d, expression of the hairpin-insensitive *MICU1* in knockdown cells was sufficient to fully restore mitochondrial Ca^{2+} uptake in sh1-*MICU1* knockdown cells. Gene expression analysis by quantitative polymerase chain reaction (qPCR) revealed that the endogenous *MICU1* expression, measured by a 3′ untranslated region (UTR)-specific assay, remained silenced, whereas the exogenous RNAi-insensitive transcript was highly expressed (Fig. 1e), demonstrating that the phenotypic rescue is attributable to exogenous expression of *MICU1*. The knockdown–phenotype correlation, combined with the cDNA rescue study, firmly establish that the observed RNAi phenotype is attributable to silencing of *MICU1* and not to an off-target effect.

Oxidative phosphorylation in *MICU1*-silenced cells

Because mitochondrial Ca^{2+} uptake is dependent on mitochondrial membrane potential (ψ_m), any defect in the electron transport chain or in membrane polarization could, in principle, give rise to a secondary defect in Ca^{2+} uptake. We therefore sought to determine whether knockdown of *MICU1* affected ψ_m or respiration in intact cells. ψ_m of *MICU1*-silenced cells was comparable to control cells, and in both cases, could be fully depolarized using the uncoupler carbonyl cyanide *m*-chlorophenylhydrazone (CCCP) (Fig. 2a). We next tested the

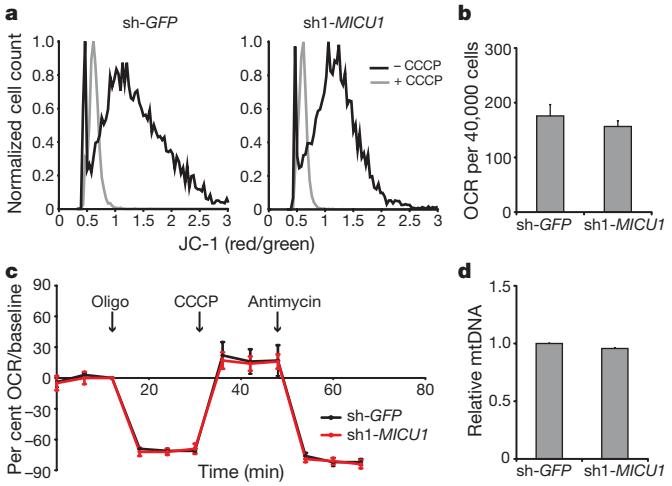

Figure 2 | Mitochondrial membrane potential, respiration and mtDNA copy number in *MICU1*-silenced cells. **a**, Mitochondrial membrane potential in *MICU1*-knockdown (sh1-*MICU1*) and control (sh-*GFP*) cells measured by JC-1 fluorescence in the presence or absence of the uncoupler CCCP (5 μM). **b**, Basal oxygen consumption rate (OCR, pmol O_2 min^{-1}) in control and knockdown cells. Error bars indicate mean ± s.d. **c**, Normalized OCR in sh1-*MICU1* and sh-*GFP* cells after the addition of the complex V inhibitor oligomycin (Oligo; 0.5 μM), uncoupler CCCP (0.5 μM), and complex III inhibitor antimycin (0.5 μM). Results are mean ± s.d. of five independent replicates. **d**, mtDNA copy number relative to nuclear DNA in *MICU1*-knockdown and control cells. Values are mean ± s.d. of three independent replicates.

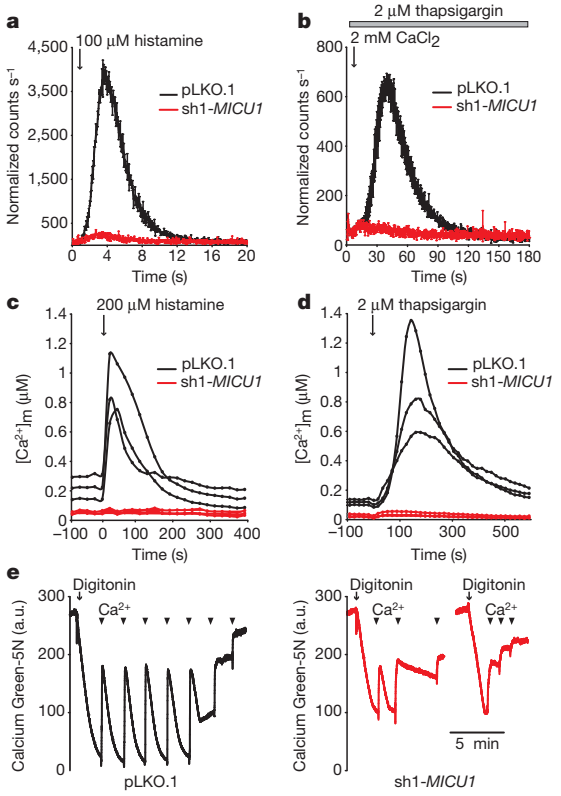

Figure 3 | Measurement of mitochondrial Ca^{2+} uptake kinetics in populations of cells, individual cells and permeabilized cells. **a**, Luminescence measurements of mitochondrial Ca^{2+} following histamine stimulation in *MICU1*-silenced (sh1-*MICU1*) and control (pLKO.1) mt-AEQ cells normalized to 30,000 cells (mean ± s.d., $n = 3$). **b**, Luminescence measurements of mitochondrial Ca^{2+} after the addition of $CaCl_2$ in cells pre-treated with thapsigargin (mean ± s.d., $n = 3$). **c**, Mitochondrial Ca^{2+} dynamics in single HeLa cells measured by FRET following treatment with histamine. Traces are representative of $n = 20$ control and $n = 12$ sh1-*MICU1* cells. **d**, Similar measurements in HeLa cells after stimulation with thapsigargin. Traces are representative of $n = 15$ control and $n = 11$ sh1-*MICU1* cells. **e**, Representative traces of mitochondrial Ca^{2+} uptake in digitonin-permeabilized mt-AEQ HeLa cells using Calcium Green-5N to measure extramitochondrial Ca^{2+}. Arrowheads denote addition of 50 μM pulses of $CaCl_2$. a.u., arbitrary units.

impact of *MICU1* knockdown on mitochondrial oxidative phosphorylation by measuring the oxygen consumption rate (OCR) of intact cells at baseline and after treatment with key electron transport chain inhibitors or uncouplers. We found that the basal respiration rate was fully preserved in sh1-*MICU1* knockdown cells (Fig. 2b). Moreover, the ATP-coupled respiratory rate, the maximal uncoupled rate, and the leak rate of respiration were similar in control and sh1-*MICU1* knockdown cells (Fig. 2c). Mitochondrial DNA (mtDNA) copy number was also unchanged (Fig. 2d). Collectively, these data demonstrate that oxidative phosphorylation is intact in *MICU1*-silenced cells and that the mitochondrial Ca^{2+} uptake phenotype is not a secondary consequence of generalized dysfunction within this organelle.

Secondary assays of Ca^{2+} homeostasis

We next performed detailed secondary analyses of Ca^{2+} homeostasis in sh1-*MICU1* knockdown cells, using multiple techniques (Fig. 3).

First, we measured mitochondrial Ca^{2+} uptake in populations of cells using two methods to mobilize Ca^{2+}. Histamine stimulation of control mt-AEQ HeLa cells (pLKO.1) resulted in typical kinetics of mitochondrial calcium uptake[3] (Fig. 3a). This uptake was impaired by silencing *MICU1*, confirming the screening result (Fig. 1). We observed the same Ca^{2+} phenotype when using store-operated Ca^{2+} entry to raise intracellular free Ca^{2+} (ref. 31). Namely, we pre-treated cells with thapsigargin, an inhibitor of the sarco-endoplasmic reticulum Ca^{2+} ATPase (SERCA) pump, in the absence of extracellular Ca^{2+} to deplete ER stores and activate store-operated Ca^{2+} channels at the plasma membrane. The re-addition of 2 mM Ca^{2+} resulted in a transient rise of $[Ca^{2+}]_m$ in control cells whereas *MICU1*-knockdown cells did not respond (Fig. 3b), consistent with the result obtained with histamine stimulation (Fig. 3a).

Second, we performed quantitative, single-cell analyses of basal $[Ca^{2+}]_m$ and agonist-stimulated rises in $[Ca^{2+}]_m$ in HeLa cells using a mitochondria-targeted calcium fluorescence resonance energy transfer (FRET) reporter[32]. We observed a significant difference in the baseline $[Ca^{2+}]_m$ in control cells versus sh1-*MICU1* knockdown cells (Table 1). Moreover, histamine treatment induced an increase in $[Ca^{2+}]_m$ in control cells (fractional saturation of 0.75 ± 0.16, $n = 20$) that was abrogated in sh1-*MICU1* cells (fractional saturation of 0.20 ± 0.10, $n = 12$) ($P < 0.0001$). Similarly, when thapsigargin was used as the calcium agonist, $[Ca^{2+}]_m$ increased in control cells (fractional saturation of 0.72 ± 0.15, $n = 15$) but did not rise in *MICU1*-silenced cells (fractional saturation of 0.10 ± 0.01, $n = 11$) ($P < 0.0001$). Representative traces from individual cells are shown in Fig. 3c, d.

Third, we measured mitochondrial Ca^{2+} uptake in digitonin-permeabilized cells. We selectively permeabilized the cell plasma membrane with a titrated amount of digitonin and monitored the clearance of exogenously added Ca^{2+} with Calcium Green-5N[33] (see Methods). Clearance of exogenous Ca^{2+} is due to uptake by energized mitochondria via the classically defined uniporter, as it is fully abrogated by the ruthenium red derivative Ru-360 or uncoupler (Supplementary Fig. 2a,b), and not influenced by thapsigargin (Supplementary Fig. 2c). Mitochondria of permeabilized control cells were capable of buffering multiple pulses of exogenously added Ca^{2+} (Fig. 3e). However, *MICU1*-silenced cells showed a strongly attenuated response, typically buffering only a single pulse (Fig. 3e).

Collectively, our secondary assays of mitochondrial Ca^{2+} uptake in cell populations and single cells with three different measurement techniques and two different Ca^{2+} agonists confirm that MICU1 is required for mitochondrial Ca^{2+} uptake in HeLa cells, and that the Ca^{2+} phenotype in *MICU1* knockdown cells is independent of the

Table 1 | Intracellular calcium measurements

Ca^{2+} measurement	pLKO.1	sh1-*MICU1*	*P*-value‡
Resting $[Ca^{2+}]_m$	0.21 ± 0.08 μM ($n = 30$)	0.04 ± 0.01 μM ($n = 25$)	<0.0001
Resting $[Ca^{2+}]_c$	0.10 ± 0.06 μM ($n = 38$)	0.08 ± 0.06 μM ($n = 40$)	0.10
Resting $[Ca^{2+}]_{ER}$*	0.69 ± 0.12 ($n = 18$)	0.68 ± 0.09 ($n = 22$)	0.99
SOCE amplitude†	0.78 ± 0.18 ($n = 21$)	0.76 ± 0.08 ($n = 21$)	0.67

* Data are reported as ΔR ($R - R_{min}$), where R is the FRET ratio.
† Store operated calcium entry (SOCE). Data are reported as a fraction of the maximum value, $(R_{SOCE} - R_{min})/(R_{max} - R_{min})$.
‡ *P*-values correspond to a two-sided Student's *t*-test with unequal variance for resting $[Ca^{2+}]_c$, resting $[Ca^{2+}]_{ER}$ and SOCE. For resting $[Ca^{2+}]_m$, the *P*-value corresponds to one-way ANOVA.

Ca^{2+} agonist or the measurement technique. Moreover, MICU1 seems to have a very specific role in mitochondrial Ca^{2+} handling, as resting ER calcium concentration ($[Ca^{2+}]_{ER}$), cytoplasmic calcium concentration ($[Ca^{2+}]_c$), and store-operated calcium entry (SOCE) rates are not significantly different between control and knockdown cells (Table 1).

MICU1 localization and domain structure

MICU1 was first identified as a 54-kDa autoantigen[34], and proteomics studies from our group and others established its mitochondrial localization in 13 different mammalian tissues[27,35]. We confirmed that MICU1 localizes predominantly to mitochondria, as a carboxy terminus GFP-tagged MICU1 exhibited clear overlap with a mitochondrial marker (Fig. 4a). We obtained similar results using a V5 epitope tag or other mitochondrial markers (MitoTracker red, Mito-HcRed) (data not shown). MICU1 has an amino-terminus mitochondrial targeting sequence followed by a predicted transmembrane domain. V5-tagged MICU1 showed progressive enrichment from crude and Percoll purified mitochondria to mitoplasts prepared from HEK293 cells (Fig. 4b), consistent with a proteomic study that localized MICU1 to the inner membrane fraction of liver mitochondria[29].

MICU1 has two canonical EF hands (EF1 and EF2) that are separated by an unusually long predicted helix (Fig. 4c). The two canonical EF hands are highly conserved in fish, flies, nematodes and kinetoplastids, even at the level of individual residues that coordinate binding to Ca^{2+}. To determine whether these EF hands are required for MICU1-mediated Ca^{2+} uptake, we created an EF mutant cell line (*MICU1mEF*). We used the sh1-insensitive cDNA construct described above (Fig. 1c) and introduced point mutations into EF1 (D231A, E242K) as well as EF2 (D421A, E432K). Although the RNAi Ca^{2+} uptake phenotype can be fully rescued by overexpression of a wild-type allele, *MICU1mEF* fails to fully restore mitochondrial Ca^{2+} uptake (Fig. 4d, e). These results demonstrate that EF hands in MICU1 are essential for mitochondrial Ca^{2+} uptake.

Role of MICU1 in metabolic coupling

Several TCA cycle dehydrogenases are known to be regulated by Ca^{2+} (refs 9,10), and conversely, studies have shown that mitochondria can shape cytosolic Ca^{2+} dynamics by buffering of intracellular free Ca^{2+} (refs 6,7). Such "coupling" by Ca^{2+} has been proposed to be an important mechanism for the regulation of Ca^{2+} signalling by the mitochondrion, as well as for balancing cytosolic ATP utilization with mitochondrial ATP production[36,37]. Given the requirement of a functional MICU1 for mitochondrial Ca^{2+} uptake, we were interested in determining whether MICU1 contributes to metabolic coupling.

First, we used a cytosolic-targeted cameleon[32] and monitored $[Ca^{2+}]_c$ rise in single cells challenged with two different Ca^{2+} agonists. As illustrated in Fig. 5a, b, both *MICU1*-knockdown and control cells responded to calcium agonists and substantially increased their $[Ca^{2+}]_c$. However, silencing of *MICU1* slowed the clearance kinetics of $[Ca^{2+}]_c$ in response to thapsigargin (53% clearance at 200 s in control cells, $n = 14$, versus 28% clearance in *MICU1*-silenced cells, $n = 16$, $P < 0.0001$) as well as in response to histamine (representative traces shown in Fig. 5b).

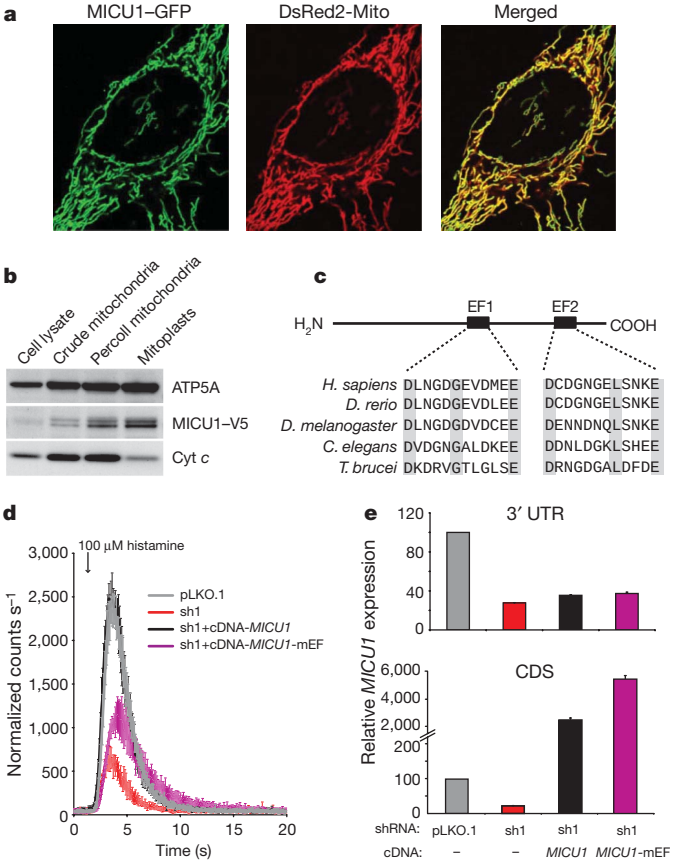

Figure 4 | MICU1 is an EF-hand protein localized to mitochondria. **a**, Confocal microscopy image of a HeLa cell expressing C-terminus GFP-tagged MICU1 and DsRed2-Mito. **b**, Immunoblot analysis of whole-cell lysates, crude mitochondria, Percoll purified mitochondria and mitoplasts isolated from HEK293 cells expressing C-terminus V5-tagged MICU1. **c**, Domain structure of MICU1 highlighting two evolutionarily conserved canonical EF hands. **d**, cDNA rescue of the sh1-*MICU1* mitochondrial Ca^{2+} uptake phenotype. Kinetic traces of mitochondrial Ca^{2+} uptake normalized to cell number are shown for control cells (pLKO.1), sh1-*MICU1* cells and sh1-*MICU1* cells rescued using a cDNA expressing a wild-type allele of *MICU1* or an EF mutant (*MICU1mEF*) (mean ± s.d., $n = 3$). **e**, Quantification of endogenous (3′ UTR) and endogenous plus exogenous (CDS) *MICU1* expression for the cDNA rescue experiment described in **d**. Relative gene expression is reported as percentage change over control cells (pLKO.1) using actin as an endogenous control (mean ± s.d., $n = 3$).

Next we sought to determine whether silencing of *MICU1* can compromise the ability of cytosolic Ca^{2+} rises to stimulate mitochondrial oxidative metabolism. We followed the activation of mitochondrial dehydrogenases after histamine stimulation by monitoring the level of NAD(P)H fluorescence in single cells (see Methods). As expected, NAD(P)H fluorescence increased upon challenge with rotenone and dropped after treatment with CCCP, indicating that the observed signal is reflective of the mitochondrial NADH pool (Supplementary Fig. 3). Treatment of control cells with histamine led to a pronounced increase in NAD(P)H fluorescence (Fig. 5c), but this rise was significantly attenuated in *MICU1*-silenced cells. Specifically, the histamine-induced elevation in NAD(P)H fluorescence was 117 ± 35 ($n = 12$) in control cells versus 58 ± 28 ($n = 24$) for *MICU1*-silenced cells ($P = 3.0 \times 10^{-6}$). Notably, control and knockdown cell lines showed a robust elevation in NAD(P)H fluorescence in response to rotenone treatment, indicating that their mitochondrial NADH pools were intact.

Collectively, our studies (Fig. 5) offer strong support for a role of MICU1 in coupling cytosolic Ca^{2+} transients and mitochondrial energy metabolism.

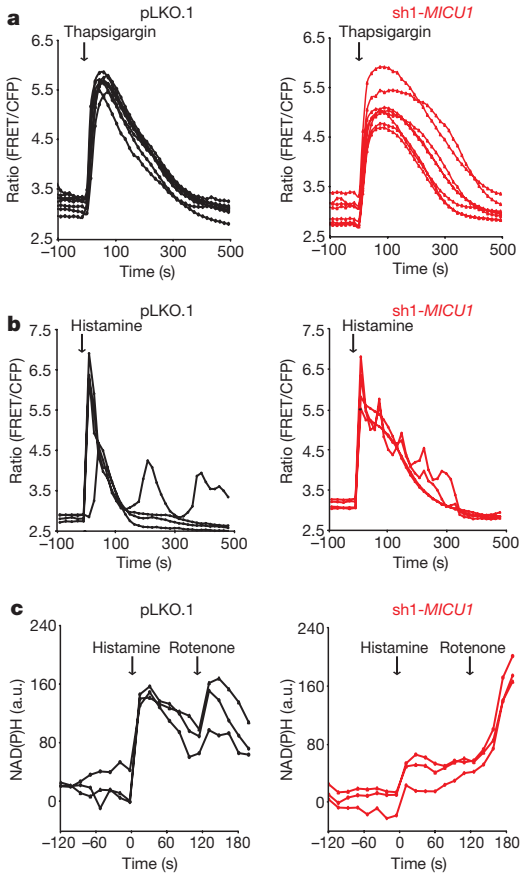

Figure 5 | Contribution of *MICU1* to cytosolic Ca^{2+} dynamics and metabolic coupling. **a**, Single-cell FRET measurements of cytosolic Ca^{2+} dynamics in *MICU1*-silenced (sh1-*MICU1*) and control (pLKO.1) HeLa cells after thapsigargin (5 μM) stimulation. Traces are representative of $n = 14$ cells for pLKO.1 and $n = 16$ cells for sh1-*MICU1* and are reported as a FRET ratio (FRET/CFP). **b**, Single-cell FRET measurements of cytosolic Ca^{2+} dynamics in *MICU1*-silenced (sh1-*MICU1*) and control (pLKO.1) HeLa cells after histamine (200 μM) stimulation. Traces are representative of $n = 28$ cells for pLKO.1 and $n = 17$ cells for sh1-*MICU1*. **c**, Single-cell measurements of NAD(P)H in sh1-*MICU1* and pLKO.1 cells. Where indicated, cells are challenged with 150 μM histamine and 2 μM rotenone. Traces are representative of $n = 12$ cells for pLKO.1 and $n = 24$ cells for sh1-*MICU1*.

Discussion

Membrane-potential-dependent uptake of Ca^{2+} by isolated mitochondria was first documented nearly 50 years ago[1,2]. Since then its biophysical properties have been extensively characterized[13,14] but so far, none of the molecular components of this high-capacity uptake machinery have been identified. Evaluating the contribution of mitochondrial Ca^{2+} uptake to intact cell physiology, growth and development has been hampered by the lack of specific and direct inhibitors[19]. Our focused RNAi screen identifies MICU1 as a key regulator of mitochondrial Ca^{2+} uptake and highlights the power of integrating genomics, RNAi and physiology. Although several mitochondrial Ca^{2+} uptake mechanisms may exist[15,20], our experimental data are consistent with a key role for MICU1 in regulating the classically defined uniporter. MICU1 localizes to mitochondria and its loss impairs mitochondrial Ca^{2+} uptake, in a manner that is dependent on its EF hands, without significantly impairing mitochondrial respiration or membrane potential. Identification of MICU1 has allowed us to provide genetic support for the contribution of mitochondrial Ca^{2+} uptake to 'metabolic coupling'.

At present the precise molecular mechanism by which MICU1 controls mitochondrial Ca^{2+} uptake remains unclear, but several possibilities exist: (1) MICU1 could constitute a pore-forming channel subunit, although it is unlikely to operate alone as a monomer in this capacity because it has at most one predicted membrane-spanning domain; (2) it could be involved in buffering mitochondrial Ca^{2+} with a secondary impact on uptake; (3) it could act as a Ca^{2+} sensor via its two canonical EF hands, and gate the activity of a partner channel. The latter hypothesis would be consistent with the long-standing observation that mitochondrial Ca^{2+} uniport is allosterically controlled by Ca^{2+} with a Hill coefficient of two[38–40]. Under this model, MICU1 would be functioning in a manner similar to what has been reported for STIM1, an EF-hand-containing protein that regulates ORAI1, a store-operated channel subunit[41].

Future experiments will be required to determine the precise molecular mechanism by which MICU1 controls mitochondrial Ca^{2+} entry. Because our work has focused only on a single cell type, it will also be important to determine whether MICU1 has a similar role in other cell types, or if redundant or alternative mechanisms are in place to confer tissue-specific control of Ca^{2+} homeostasis[42,43]. Regardless, the identification of MICU1 should facilitate the full molecular characterization of the mitochondrial Ca^{2+} uptake machinery, and importantly, paves the way for rigorously understanding and targeting mitochondrial Ca^{2+} uptake in normal physiology and disease.

METHODS SUMMARY

Candidate human genes required for mitochondrial Ca^{2+} uptake were prioritized based on the expression of their homologues across mouse tissues[27], localization to the inner mitochondrial membrane[28,29], and evolutionary conservation in kinetoplastids[22–24] but not in the yeast *S. cerevisiae*[22,25,26]. A focused RNAi screen was performed against 13 human genes in a commercially available, HeLa cell line expressing a mitochondria-targeted aequorin (mt-AEQ, Aequotech catalogue number AT-002-H) using lentiviral constructs available from the Broad Institute's RNAi Consortium[44]. cDNA rescue studies in *MICU1* knockdown cells were carried out by overexpression of a custom synthesized cDNA containing synonymous mutations at all eight codons complementary to the strongest hairpin as well as point mutations in the two EF hands (Blue Heron Biotechnology). Agonist-induced rises in mitochondrial Ca^{2+} were measured in mt-AEQ HeLa cells by luminescence[30,31]. FRET-based measurements of mitochondrial, cytosolic and ER Ca^{2+} in single HeLa cells were performed using the 4mtD3cpv, D3cpv and D1ER FRET sensors, respectively[32]. Measurements of Ca^{2+} uptake in permeabilized HeLa cells were made using Calcium Green-5N[33]. Mitochondrial respiration, morphology and mtDNA copy number were measured as previously described[45]. Mitochondrial membrane potential was measured by flow cytometry on cells stained with JC-1 according to the manufacturer's protocol. Single-cell measurements of NAD(P)H were performed via established protocols[46]. Crude mitochondria, Percoll-purified mitochondria and mitoplasts were prepared from cultured HEK293 cells expressing a C-terminus V5 tagged version of MICU1[47,48]. Unless otherwise indicated, data are summarized as mean ± standard deviation, and *P*-values were computed from *t*-tests.

Full Methods and any associated references are available in the online version of the paper at www.nature.com/nature.

Received 10 March; accepted 19 July 2010.
Published online 8 August 2010.

1. DeLuca, H. F. & Engstrom, G. W. Calcium uptake by rat kidney mitochondria. *Proc. Natl Acad. Sci. USA* **47**, 1744–1750 (1961).
2. Vasington, F. D. & Murphy, J. V. Ca ion uptake by rat kidney mitochondria and its dependence on respiration and phosphorylation. *J. Biol. Chem.* **237**, 2670–2677 (1962).
3. Rizzuto, R., Simpson, A. W., Brini, M. & Pozzan, T. Rapid changes of mitochondrial Ca^{2+} revealed by specifically targeted recombinant aequorin. *Nature* **358**, 325–327 (1992).
4. Filippin, L., Magalhaes, P. J., Di Benedetto, G., Colella, M. & Pozzan, T. Stable interactions between mitochondria and endoplasmic reticulum allow rapid accumulation of calcium in a subpopulation of mitochondria. *J. Biol. Chem.* **278**, 39224–39234 (2003).
5. Palmer, A. E. *et al.* Ca^{2+} indicators based on computationally redesigned calmodulin-peptide pairs. *Chem. Biol.* **13**, 521–530 (2006).
6. Jouaville, L. S., Ichas, F., Holmuhamedov, E. L., Camacho, P. & Lechleiter, J. D. Synchronization of calcium waves by mitochondrial substrates in *Xenopus laevis* oocytes. *Nature* **377**, 438–441 (1995).
7. Kaftan, E. J., Xu, T., Abercrombie, R. F. & Hille, B. Mitochondria shape hormonally induced cytoplasmic calcium oscillations and modulate exocytosis. *J. Biol. Chem.* **275**, 25465–25470 (2000).

8. Spat, A., Szanda, G., Csordas, G. & Hajnoczky, G. High- and low-calcium-dependent mechanisms of mitochondrial calcium signalling. *Cell Calcium* **44,** 51–63 (2008).
9. Denton, R. M. & McCormack, J. G. The role of calcium in the regulation of mitochondrial metabolism. *Biochem. Soc. Trans.* **8,** 266–268 (1980).
10. Hajnoczky, G., Robb-Gaspers, L. D., Seitz, M. B. & Thomas, A. P. Decoding of cytosolic calcium oscillations in the mitochondria. *Cell* **82,** 415–424 (1995).
11. Balaban, R. S. The role of Ca^{2+} signaling in the coordination of mitochondrial ATP production with cardiac work. *Biochim. Biophys. Acta* **1787,** 1334–1341 (2009).
12. Bernardi, P. & Rasola, A. Calcium and cell death: the mitochondrial connection. *Subcell. Biochem.* **45,** 481–506 (2007).
13. Gunter, K. K. & Gunter, T. E. Transport of calcium by mitochondria. *J. Bioenerg. Biomembr.* **26,** 471–485 (1994).
14. Kirichok, Y., Krapivinsky, G. & Clapham, D. E. The mitochondrial calcium uniporter is a highly selective ion channel. *Nature* **427,** 360–364 (2004).
15. Santo-Domingo, J. & Demaurex, N. Calcium uptake mechanisms of mitochondria. *Biochim. Biophys. Acta* **1797,** 907–912 (2010).
16. Mironova, G. D. *et al.* Isolation and properties of Ca^{2+}-transporting glycoprotein and peptide from beef heart mitochondria. *J. Bioenerg. Biomembr.* **14,** 213–225 (1982).
17. Panfili, E. *et al.* Specific inhibition of mitochondrial Ca^{2+} transport by antibodies directed to the Ca^{2+}-binding glycoprotein. *Nature* **264,** 185–186 (1976).
18. Zazueta, C., Zafra, G., Vera, G., Sanchez, C. & Chavez, E. Advances in the purification of the mitochondrial Ca^{2+} uniporter using the labeled inhibitor 103Ru360. *J. Bioenerg. Biomembr.* **30,** 489–498 (1998).
19. Hajnóczky, G. *et al.* Mitochondrial calcium signalling and cell death: approaches for assessing the role of mitochondrial Ca^{2+} uptake in apoptosis. *Cell Calcium* **40,** 553–560 (2006).
20. Sparagna, G. C., Gunter, K. K., Sheu, S. S. & Gunter, T. E. Mitochondrial calcium uptake from physiological-type pulses of calcium. A description of the rapid uptake mode. *J. Biol. Chem.* **270,** 27510–27515 (1995).
21. Jiang, D., Zhao, L. & Clapham, D. E. Genome-wide RNAi screen identifies Letm1 as a mitochondrial Ca^{2+}/H^{+} antiporter. *Science* **326,** 144–147 (2009).
22. Carafoli, E. & Lehninger, A. L. A survey of the interaction of calcium ions with mitochondria from different tissues and species. *Biochem. J.* **122,** 681–690 (1971).
23. Docampo, R. & Vercesi, A. E. Ca^{2+} transport by coupled *Trypanosoma cruzi* mitochondria *in situ*. *J. Biol. Chem.* **264,** 108–111 (1989).
24. Vercesi, A. E. & Docampo, R. Ca^{2+} transport by digitonin-permeabilized Leishmania donovani. Effects of Ca^{2+}, pentamidine and WR-6026 on mitochondrial membrane potential *in situ*. *Biochem. J.* **284,** 463–467 (1992).
25. Balcavage, W. X., Lloyd, J. L., Mattoon, J. R., Ohnishi, T. & Scarpa, A. Cation movements and respiratory response in yeast mitochondria treated with high Ca^{2+} concentrations. *Biochim. Biophys. Acta* **305,** 41–51 (1973).
26. Uribe, S., Rangel, P. & Pardo, J. P. Interactions of calcium with yeast mitochondria. *Cell Calcium* **13,** 211–217 (1992).
27. Pagliarini, D. J. *et al.* A mitochondrial protein compendium elucidates complex I disease biology. *Cell* **134,** 112–123 (2008).
28. Da Cruz, S. *et al.* Proteomic analysis of the mouse liver mitochondrial inner membrane. *J. Biol. Chem.* **278,** 41566–41571 (2003).
29. McDonald, T. *et al.* Expanding the subproteome of the inner mitochondria using protein separation technologies: one- and two-dimensional liquid chromatography and two-dimensional gel electrophoresis. *Mol. Cell. Proteomics* **5,** 2392–2411 (2006).
30. Brini, M., Pinton, P., Pozzan, T. & Rizzuto, R. Targeted recombinant aequorins: tools for monitoring $[Ca^{2+}]$ in the various compartments of a living cell. *Microsc. Res. Tech.* **46,** 380–389 (1999).
31. Glitsch, M. D., Bakowski, D. & Parekh, A. B. Store-operated Ca^{2+} entry depends on mitochondrial Ca^{2+} uptake. *EMBO J.* **21,** 6744–6754 (2002).
32. Palmer, A. E. & Tsien, R. Y. Measuring calcium signaling using genetically targetable fluorescent indicators. *Nature Protocols* **1,** 1057–1065 (2006).
33. Murphy, A. N., Bredesen, D. E., Cortopassi, G., Wang, E. & Fiskum, G. Bcl-2 potentiates the maximal calcium uptake capacity of neural cell mitochondria. *Proc. Natl Acad. Sci. USA* **93,** 9893–9898 (1996).
34. Aichberger, K. J. *et al.* Hom s 4, an IgE-reactive autoantigen belonging to a new subfamily of calcium-binding proteins, can induce Th cell type 1-mediated autoreactivity. *J. Immunol.* **175,** 1286–1294 (2005).
35. Forner, F. *et al.* Proteome differences between brown and white fat mitochondria reveal specialized metabolic functions. *Cell Metab.* **10,** 324–335 (2009).
36. Jouaville, L. S., Pinton, P., Bastianutto, C., Rutter, G. A. & Rizzuto, R. Regulation of mitochondrial ATP synthesis by calcium: evidence for a long-term metabolic priming. *Proc. Natl Acad. Sci. USA* **96,** 13807–13812 (1999).
37. Territo, P. R., Mootha, V. K., French, S. A. & Balaban, R. S. Ca^{2+} activation of heart mitochondrial oxidative phosphorylation: role of the F_0/F_1-ATPase. *Am. J. Physiol. Cell Physiol.* **278,** C423–C435 (2000).
38. Bragadin, M., Pozzan, T. & Azzone, G. F. Kinetics of Ca^{2+} carrier in rat liver mitochondria. *Biochemistry* **18,** 5972–5978 (1979).
39. Igbavboa, U. & Pfeiffer, D. R. EGTA inhibits reverse uniport-dependent Ca^{2+} release from uncoupled mitochondria. Possible regulation of the Ca^{2+} uniporter by a Ca^{2+} binding site on the cytoplasmic side of the inner membrane. *J. Biol. Chem.* **263,** 1405–1412 (1988).
40. Moreau, B., Nelson, C. & Parekh, A. B. Biphasic regulation of mitochondrial $Ca^{2}+$ uptake by cytosolic Ca^{2+} concentration. *Curr. Biol.* **16,** 1672–1677 (2006).
41. Zhang, S. L. *et al.* STIM1 is a Ca^{2+} sensor that activates CRAC channels and migrates from the Ca^{2+} store to the plasma membrane. *Nature* **437,** 902–905 (2005).
42. Lawrie, A. M., Rizzuto, R., Pozzan, T. & Simpson, A. W. A role for calcium influx in the regulation of mitochondrial calcium in endothelial cells. *J. Biol. Chem.* **271,** 10753–10759 (1996).
43. Favaron, M. & Bernardi, P. Tissue-specific modulation of the mitochondrial calcium uniporter by magnesium ions. *FEBS Lett.* **183,** 260–264 (1985).
44. Moffat, J. *et al.* A lentiviral RNAi library for human and mouse genes applied to an arrayed viral high-content screen. *Cell* **124,** 1283–1298 (2006).
45. Gohil, V. M. *et al.* Nutrient-sensitized screening for drugs that shift energy metabolism from mitochondrial respiration to glycolysis. *Nature Biotechnol.* **28,** 249–255 (2010).
46. Gaspers, L. D. & Thomas, A. P. Calcium-dependent activation of mitochondrial metabolism in mammalian cells. *Methods* **46,** 224–232 (2008).
47. Mootha, V. K. *et al.* Integrated analysis of protein composition, tissue diversity, and gene regulation in mouse mitochondria. *Cell* **115,** 629–640 (2003).
48. Mootha, V. K. *et al.* A reversible component of mitochondrial respiratory dysfunction in apoptosis can be rescued by exogenous cytochrome c. *EMBO J.* **20,** 661–671 (2001).

Supplementary Information is linked to the online version of the paper at www.nature.com/nature.

Acknowledgements We thank Z. Grabarek, S. Silver and D. Root for advice; S. Calvo and A. Wolf for assistance with bioinformatics; P. Federico for technical assistance; and members of the Mootha Laboratory for valuable feedback. This work was supported by grants from the National Institutes of Health (GM084027) to A.E.P, TR2 GM08759 to J.E.M. and GM0077465, DK080261 awarded to V.K.M., and by an HHMI Early Career Physician Scientist Award to V.K.M.

Author Contributions F.P. and V.K.M conceived of the project and its design. F.P., V.M.G., H.S.G., X.R.B., J.E.M. and A.E.P. performed experiments and data analysis. F.P. and V.K.M. wrote the manuscript.

Author Information Reprints and permissions information is available at www.nature.com/reprints. The authors declare no competing financial interests. Readers are welcome to comment on the online version of this article at www.nature.com/nature. Correspondence and requests for materials should be addressed to V.K.M. (vamsi@hms.harvard.edu).

METHODS

Prioritization of candidate genes. We used previously published data sets to prioritize candidate genes that are required for mitochondrial Ca^{2+} uptake[27–29]. We found that 18 human genes (*SQRDL*, *CBARA1* (*MICU1*), *GPAM*, *HADH*, *NDUFV1*, *NDUFA9*, *STOML2*, *NDUFA13*, *DCI*, *NDUFB9*, *NDUFS7*, *ACADL*, *ACADM*, *ACADVL*, *OXCT1*, *NDUFV2*, *PTGES2*, *NDUFS1*) met the requirements for (1) a reliable mitochondrial localization based on our previously published MitoCarta inventory of 1,098 mouse mitochondrial proteins[27] (1,013 human homologues) (http://www.broad.mit.edu/publications/MitoCarta); (2) association with the mitochondrial inner membrane based on proteomic studies of mouse and rat liver mitochondria[28,29] (225 of 1,013); (3) evolutionary conservation in kinetoplastids but not in the yeast *S. cerevisiae* (58 of 1,013) according to our previously published phylogenetic analysis[27]; and (4) protein expression across at least 10 mouse tissues (616 of 1,013) based on our mitochondrial tissues atlas[27]. Of these, 5 genes (*ACADL*, *ACADM*, *ACADVL*, *OXCT1*, *PTGES2*) either had obvious roles in other pathways or did not have readily available RNAi reagents and were therefore not pursued.

Cell culture. HeLa cells expressing a commercially available mitochondrial matrix targeted aequorin (mt-AEQ; Aequotech catalogue no. AT-002-H) were grown in DMEM (Invitrogen catalogue no. 11995) supplemented with 10% FBS (Gibco catalogue no. 16000) and 100 μg ml^{-1} geneticin (Gibco catalogue no. 10131-035) at 37 °C and 5% CO_2. mt-AEQ HeLa cells expressing gene-specific lentiviral shRNAs were grown in DMEM, 10% FBS, 100 μg ml^{-1} geneticin and 2 μg ml^{-1} puromycin (Sigma catalogue no. P9620).

RNA interference screen. A library of shRNA lentiviral particles targeting our 13 candidate genes and negative controls were purchased from the Broad Institute's RNAi Consortium. Two independent screens were performed. Briefly, 15,000 mt-AEQ HeLa cells were seeded in a 96-well plate (PerkinElmer catalogue no. 6005181). After 12 h the media was replaced with DMEM supplemented with 10% FBS and 8 μg ml^{-1} polybrene (Sigma catalogue no. H9268). Infection was performed by addition of 20 μl of gene-specific shRNA lentivirus suspension to each well followed by 30 min of centrifugation at 800*g* at 37 °C. Cells were washed three times with regular growth media and returned to 37 °C at 5% CO_2. Twenty-four hours after infection, infected cells were selected in growth media supplemented with 2 μg ml^{-1} puromycin. Luminescence-based measurements of mitochondrial Ca^{2+} and cell number were performed 6 days after infection. Cell number and viability were assayed by CellTiter-Glo Luminescent Viability assay (Promega catalogue no. G7571).

cDNA rescue experiments. A version of *MICU1* cDNA resistant to sh1-*MICU1* knockdown was *de novo* synthesized (Blue Heron Biotechnology) and cloned into a pENTR221 vector, ready for use in the Gateway cloning system (Invitrogen). The cDNA harboured eight synonymous mutations in the codons complementary to sh1-*MICU1*. Similarly, a mutated version of sh1-*MICU1* insensitive cDNA was *de novo* synthesized which harbours two point mutations into the first EF hand domain, EF1 (D231A, E242K), as well as two mutations in the second EF hand domain, EF2 (D421A, E432K), to create a *MICU1* EF mutant (*MICU1mEF*). Procedures and reagents for virus production and infection have been previously published[44]. Twenty-four hours after infection sh1-*MICU1* knockdown cells expressing sh1-*MICU1*-resistant cDNAs were selected with 2 μg ml^{-1} puromycin (Sigma P9620) and 10 μg ml^{-1} blasticidin (Invitrogen A11139).

Luminescence measurement of mitochondrial Ca^{2+}. Measurements of mitochondrial Ca^{2+} were performed upon both histamine and thapsigargin treatment as described previously[30, 31]. Light emission was measured in a luminescence counter (MicroBeta^2 LumiJET Microplate Counter PerkinElmer) at 469 nm every 0.1 s.

Assays of mitochondrial membrane potential, respiration and mtDNA abundance. Mitochondrial respiration and mtDNA copy number were measured as previously described[45]. Mitochondrial membrane potential was measured by flow cytometry (BD Biosciences LSR II flow cytometer) using cells stained with JC-1 according to the manufacturer's protocol. JC-1 was excited at 488 nm, green fluorescence was quantified between 515 and 545 nm, and red fluorescence was quantified between 562 and 588 nm.

Measurement of mitochondrial Ca^{2+} uptake in digitonin-permeabilized cells. Extramitochondrial free Ca^{2+} was monitored in the presence of digitonin-permeabilized cells as described previously[33]. Briefly, 2×10^6 cells were resuspended in KCl medium (125 mM KCl, 2 mM K_2HPO_4, 1 mM $MgCl_2$, 20 mM HEPES, pH 7.4) containing 5 mM glutamate, 5 mM malate and 5 mM succinate as respiratory substrates and 0.8 μM Calcium Green-5N. The plasma membranes were then selectively permeabilized with digitonin (0.01% wt/vol). Fluorescence (Ex. 506/Em. 531 nm) was monitored at 27 °C using a PerkinElmer LS-50B fluorescence spectrophotometer equipped with a stirring device.

FRET-based measurement of mitochondrial, cytosolic and ER Ca^{2+}. Cytosolic, mitochondrial and ER Ca^{2+} levels were measured using the D3cpv, 4mtD3cpv and D1ER Ca^{2+} sensors, respectively[32]. Briefly, cells were seeded on 3.5-cm imaging dishes, transiently transfected using TransIt (Mirus) according to manufacturer's protocol, and imaged 48 h after transfection. Imaging experiments were performed on an Axiovert 200M inverted fluorescence microscope (Zeiss) with a Cascade 512B CCD camera (Roper scientific), and equipped with CFP (430/24 excitation, 455 dichroic, 470/24 emission), YFP (495/10 excitation, 515 dichroic, 535/25 emission) and FRET (430/24 excitation, 455 dichroic, 535/25 emission) filters controlled by a Lambda 10-3 filter changer (Sutter Instruments) and analysed using Metafluor software (Universal Imaging). Details on the microscope, sensor calibration and conversion of FRET ratios (including protocol for obtaining R_{min} and R_{max}) into Ca^{2+} concentrations have been published[32]. Statistical significance was evaluated using either Student's *t*-test or two sample ANOVA.

Microscopy-based NAD(P)H measurements. Measurement of cellular NAD(P)H was carried out according to established protocols[46]. Briefly, cells were treated with histamine (150 μM), followed by rotenone (2 μM). The NAD(P)H signal was measured with the following settings: 380/10 excitation filter, 455 dichroic, 475/24 emission filter, and 0.6 (25% transmission) neutral density filter, and 1,000 ms exposure time.

Isolation of mitochondria and western blot analysis. Cell lysates, crude and Percoll purified mitochondria were prepared from cultured HEK293 cells[47]. Percoll purified mitochondria (0.2 mg) were hypotonically lysed as previously described[48]. Immunoblotting of the four fractions (5 μg) was performed with commercially available antibodies: anti-cytochrome *c* (Mitoscience, MSA06), anti-ATP synthase subunit α (Mitoscience, MS502) and anti-V5 antibody (Invitrogen, R96025).